IEEE ComSoc IEEE Communications Society
IEEE Open Journal of the Communications Society

Received 5 December 2023; revised 20 December 2023; accepted 21 December 2023. Date of publication 5 January 2024; date of current version 29 January 2024.

Digital Object Identifier 10.1109/OJCOMS.2024.3350511

An Energy-Efficient Cluster Formation Based on Optimal Node Distribution in Full Capacity Multi-Hop LoRa Networks

BISWAJIT PAUL[1], CHADI ASSI[1] (Fellow, IEEE), GEORGES KADDOUM[2] (Senior Member, IEEE), RAJESH PALIT[3] (Member, IEEE), AND SALEKUL ISLAM[4] (Senior Member, IEEE)

[1]Department of Electrical and Computer Engineering, Concordia University, Montreal, QC H3G 1M8, Canada
[2]Institute for Information Systems Engineering, Concordia University, Montreal, QC H3G 1M8, Canada
[2]Department of Electrical Engineering, Ecole de Technologie Superieure, Montreal, QC H3C 1K3, Canada
[3]Department of Electrical and Computer Engineering, North South University, Dhaka 1229, Bangladesh
[4]Department of Computer Science and Engineering, United International University, Dhaka 1212, Bangladesh

CORRESPONDING AUTHOR: C. ASSI (e-mail: chadi.assi@concordia.ca)

This work was supported by the Institute for Advanced Research (IAR) Publication Grant of United International University under Grant IAR-2024-Pub-003.

ABSTRACT Our most recent findings on multi-hop LoRa networks imply that earlier developed multi-hop routing methods, such as our previously suggested Extended-DRESG scheme, had overlooked some essential information. Although the researchers employed uniform node distributions for their multi-hop models, a full capacity LoRa network may be treated as a Gaussian distribution. Extended-DRESG performs better with a Gaussian distribution than with a uniform distribution of nodes. In contrast to optimal ring-hop combinations created earlier, this observation led to the suggested algorithm for optimal ring positioning and ring-hop combinations in Extended-DRESG. The Extended-DRESG cluster developing technique, which may produce much superior performance in terms of energy efficiency when uniform node distribution is encountered, is further suggested in light of the observations made in this research. Future multi-hop models can benefit from the current observations in two ways: (i) a better understanding of the packet forwarding structure, and (ii) a good cluster formation technique when clusters are established based on their distances from the gateway.

INDEX TERMS LPWAN, WSN, routing, energy-efficient, node-distribution.

I. INTRODUCTION

LORAWAN is a promising non-cellular-based IoT network solution for many potential applications that include agriculture, inventory management, waste management, environment monitoring, and object tracking [1], [2]. Typically, LoRaWAN targets low data rate applications with less frequent message transmissions from end nodes. Some LoRaWAN applications can be found in [3], [4], [5], [6], [7], [8], [9], [10], [11]. For instance, a thousand nodes were deployed by Smart Harbours to track vehicles and assets [7]. The authors of [8] provided an example of how LoRaWAN is used in the flower industry, where a single gateway (GW) may accommodate up to 6,000 nodes (trolleys), all of which must be connected to a server while traveling around an auction floor. LoRa technology can provide access to as many as 6,000 nodes in a minute cycle time with the right scheduling of time, frequency, and spreading factors (SFs) [9]. LoRa technology for vehicle communication and indoor remote health was assessed in [10] and [11]. Researchers predict significant growth in the number of connected IoT devices soon.

The topology of LoRaWAN is star-of-stars. End nodes in LoRaWAN communicate with the GWs, and the GWs are further connected with the backend server of a cloud network. End nodes can use either LoRa channels or Gaussian frequency shift keying (GFSK) channels, and different bandwidth options are supported for LoRa channels. Six out of seven SFs can be used for uplink communication, which helps combat interference. Data rates ranging from 300 bps to 50 kbps can be supported. Different coding rates are used to enable forward error correction. Detail specifications on LoRaWAN can be obtained from [12].

Based on geographical locations, there could be some restrictions on the availability of a particular channel. There is no other restriction on communication between end nodes and the GWs. Thus, communication in LoRaWAN is similar to ALOHA [13]. An Interesting discussion on Slotted Aloha (S-ALOHA) can be found in [14]. The authors in [15] claimed that the 15 km range could be achieved with LoRaWAN in rural environments, whereas the 5 km range can be achieved in urban environments. The maximum transmission range of an end node depends on the transceiver, path loss, SFs, and transmission power (TP).

Scalability and localization for LoRaWAN have received a lot of attention in several research studies [16], [17], [18], [19], [20], [21], [22], [23]. Enhancing network performance has been the main strategy used to address network scalability. As an example, a method to lower the likelihood of packet collisions was proposed in [18] to increase network scalability. Nevertheless, the LoRa network's true capacity is rarely taken into account, which could have changed the findings of the study. This is due to the fact that node distributions in a full-capacity LoRa network restrict the options for configuration parameters, like SF and TP, that nodes can select depending on their location in reference to the GW.

Consider the SF allocation approaches that have been suggested in the literature. The schemes for allocating SFs are categorized in [19], [20]. Combining the classifications suggested in [19], [20], SF allocations can be fixed [24], random [25], distance-based [26], [27], [28], ML-based, optimization-based [29], fairness-based [27], or PHY-based [26]. The explanations contained in [19], [20] indicate that these commonly adopted methods will likely go against the optimal LoRaWAN node distribution constraints. A LoRa network can be thought of as being divided into distinct regions by some concentric circles around the GW, where the radius of a concentric circle is the maximum transmission range achieved with a specific bandwidth/SF option [30]. The majority of nodes must be located close to the GW because low SFs are capable of supporting a large number of nodes because they require less Time on Air (ToA) [13]. To put it another way, achieving maximum network capacity with a uniform node distribution across the network is not possible unless LoRaWAN coverage is significantly reduced.

Uniformly distributed LoRa networks are used in the vast majority of the research articles in the literature. For instance, the authors in [31] handled the requirement for the reassignment of parameters (SF and TP) utilizing a distributed No-Regret Learning technique to accommodate the varying channel conditions. However, the nodes are considered to be uniformly distributed for a coverage radius of 2 km and 4 km, which raises concerns as we consider full network coverage or capacity. The remote nodes are likely to experience a higher risk of outages and packet collisions due to the nodes' capacity to choose the parameters selfishly. Driven by numerous smart city applications, a dense LoRa-implemented IoT network accessed by several GWs is taken into consideration in [32]. The authors assume that each GW serves a subset of uniformly distributed nodes. A highly dense network may not always follow a uniform distribution, especially for a large coverage. While some studies take into account non-uniform distributions [18], [33], concave and convex LoRaWAN deployments in [18] are the most pertinent to our investigation. However, these deployment approaches do not deal with the limitations of an optimal (full capacity and maximum coverage) LoRa network. In this research, we demonstrate how the full capacity LoRa network requirements can be satisfied using the Gaussian distribution with a suitable choice of mean and standard deviation.

Single-hop routing is currently advised for LoRa networks. The possibility of multi-hop routing being more energy-efficient was disregarded to prevent significant computational complexity at the end nodes. Furthermore, in a number of non-line-of-sight or large-scale deployment scenarios, such as underground deployment or large-scale military launch [34], the single-hop topology might not be sufficient. For instance, the transmission range of a pervasive monitoring system installed in a subterranean setting [35] was significantly reduced to less than 200 meters. The addition of GWs decreases information sharing and complicates deployment. For wireless sensor networks (WSNs), a number of multi-hop routing algorithms have been presented thus far [36], [37]. However, the low-cost requirement at the end devices (EDs) makes the adoption of those schemes infeasible in Low Power Wide Area Networks (LPWANs). Some insights on multi-hop routings in LPWANs were developed in [38]. Additional relevant papers that address the viability and possible advantages of multi-hop routing in LoRaWAN may be found in [39], [40]. Relay nodes allow nodes to employ short SFs, which lowers and balances their energy consumption, according to the authors' findings in [32]. Larger node energy reductions are achieved at the cost of increased network energy consumption when there are more relay tiers. The multi-hop routing protocol MLoRa [34] uses some EDs as relay nodes (RNs) instead of relay nodes. A clustering-based approach for multi-hop LoRa networks was proposed in [41] to enhance coverage, where nodes in different sub-nets used different SFs to enable concurrent transmission. However, the authors in [42] proposed using additional GWs in a multi-hop setting to relay data instead of using ordinary LoRa nodes to improve coverage. Some other works on multi-hop routing can be found in [43], [44], [45], [46].

We proposed a multi-hop routing scheme (Extended-DRESG) for LoRa networks in [47]. In that scheme, the ideal packet relay structure to reduce the energy consumption of the important nodes was determined by ring-hop combinations. Instead of using a uniform distribution of nodes like in [47], this research used a Gaussian distribution, which significantly improved energy efficiency over single-hop routing. We illustrate the relationship between packet forwarding structure, transmit current usage, and

ring location to learn how cluster formation affects energy consumption. Transmit current usage in accordance with the multi-hop routing scheme in [47] is based on the transmit distance ascertained by the ring positions and the hop counts. However, the number of relay packets generated by the packet forwarding structure emerging from cluster formation determines the feasible node-to-node association among clusters, and consequently, determines the nodes' energy consumption (please check Section III). This work presents an algorithm to determine the best ring placements and ring-hop combinations. Keep in mind that we might not always need the maximum coverage or full capacity, and in certain cases, uniform distribution might be appropriate. Thus, a novel cluster formation method is proposed, which can greatly increase energy efficiency for uniformly distributed nodes.

The contributions of this paper are as follows:

First, we show that a Gaussian distribution with appropriately selected parameters can closely replicate the optimal LoRaWAN node distribution scenario. An alternative approach is presented as well.

Second, we reevaluate the Extended-DRESG multi-hop routing scheme in [47] by considering the optimal LoRaWAN node distribution. The mathematical analysis visualizes the contributing factors in determining the critical nodes' energy consumption. Since fewer packets are forwarded by packet-forwarding nodes, the critical nodes' energy consumption can be effectively reduced.

Third, we develop an algorithm to find the optimal ring positions and ring-hop combinations.

Fourth, a new cluster formation scheme is proposed for uniformly distributed nodes that will replicate the packet forwarding structure observed with Gaussian distribution. Simulation results confirm the superior performance of Extended-DRESG with the proposed cluster formation scheme for uniform node distribution scenarios.

The rest of the paper is organized in the following manner: LoRaWAN in the context of 6G is explained in Section II. LoRaWAN network scalability and node distribution are discussed in Section III. Section IV analyzes the packet forwarding structure for different ring-hop combinations in the multi-hop routing scheme in [47]. In Section V, an algorithm is presented to find the optimal ring positioning and ring-hop combination. In Section VI, a novel cluster formation technique is presented for multi-hop routing. Node distribution in single-hop routing is discussed in Section VII. Simulation results are discussed in Section VIII, and conclusions are drawn in Section IX.

II. LORAWAN IN THE CONTEXT OF 6G

Networks with wireless access are essential for the mass adoption of IoT devices. IoT technologies are commonly categorized into three types based on their coverage range: short-range, medium-range, and long-range. The long-range technologies can be further classified into two groups: (i) solutions over licensed spectrum, such as NB-IoT and LTE category M, and (ii) solutions over unlicensed spectrum, such as LoRa and SigFox. A brand-new class of networks known as non-terrestrial networks (NTNs) offers incredibly broad coverage in three dimensions (3D). Among the available wireless access solutions, both Bluetooth and Bluetooth low-energy (BLE) are well-suited for short-range consumer IoT applications. BLE is primarily intended for wearables in health and fitness, as well as for smart home appliances. Zigbee works well for medium-range IoT applications, such as energy management, home automation, and smart lighting. Existing technologies in the unlicensed spectrum (i.e., LoRa, SigFox) are suitable for low-cost deployments, remote connectivity, etc., for example, IoT-enabled smart agriculture.

A billion IoT devices are still linked to the legacy 2G and 3G networks as of right now, and the number of broadband IoT devices being linked to 4G networks is rapidly rising. However, for massive IoT devices requiring low power and larger coverage—NB-IoT and LTE-M were launched. Major massive machine-type communications (mMTC) criteria, such as long battery life and high density devices in a cell, are supported by NB-IoT, which also expands coverage beyond current cellular technology. Three prominent use cases, i.e., ultra-reliable low-latency communications (URLLC), mMTC, and enhanced mobile broadband (eMBB), were considered in 5G. Note that a great deal of work still needs to be done for 6G, and that only a portion of Industry 4.0 use cases can be addressed by the key performance indicators (KPIs) available for 5G [48]. 6G is anticipated to improve 5G's spectrum and energy efficiency, enabling new services like network-connected drones, tactile Internet, and real-time augmented reality glasses.

The notion of WSN has been expanded upon by a number of current unlicensed band technologies, including Zigbee and LoRa networks, to enable low-power mesh networks among inexpensive sensors. Two popular LPWAN IoT solutions across the unlicensed spectrum are LoRa and SigFox. Although unlicensed spectrum communications reliability is a significant concern, a simplified connection has several advantages, including lower device costs, longer device battery life, and less expensive IoT network implementation. It is important to remember that the energy required for cellular network synchronization, connection formation, and signaling is on par with or even higher than the energy required for actual unlicensed spectrum data transfer. It is anticipated that cellular and LPWAN IoT solutions operating in the unlicensed spectrum will split 60 percent of the IoT market between them [48].

The use of multi-hop relay user equipments (UEs) for traffic relaying between distant UEs and a gNB should be supported by the 5G system, according to 3GPP Release 17 [49]. A use case was also presented in [49], where the company uses remote-controlled and semi-autonomous robots for most of the movement, storage, and inspection of drums (containers of chemicals) between several warehouses and the factory floor itself to minimize the risk to personnel. These articulated arm robots can be used to remotely operate

tools and items utilizing 3-D vision by a trained operator wearing specialized augmented reality goggles. A large portion of the job is completed inside metal enclosures that can stop possible chemical leaks. Signal propagation is made challenging and unexpected by the metallic enclosure walls and the drums, which also function as electromagnetic shields. The factory owner may decide to use UEs with multi-hop relay capabilities to relay messages between distant UEs and gNBs instead of setting up numerous gNBs. Even while not every UE can be used as a relay, the abundance of UEs of various kinds—mounted on cars, handheld, and on drums—guarantees enough coverage for everyone. According to the report in [49], the 5G network will offer appropriate application programming interfaces (APIs) to enable a reliable third party to keep an eye on the locations, registration status, and lifecycle of its own UEs. In order for this condition to be applicable to remote UE cases, the existing requirements need upgrade regardless of hop count. On the other hand, WSN research and development are still ongoing, with a particular emphasis on applying device-to-device (D2D) relaying in sensor network topologies [48]. There are some articles, such as [50], [51], that addressed the uniform quality of service (QoS) requirements in a WSN. Future WSNs are expected to have a diverse range of sensors with varying needs for QoS and battery life [48].

6G will be an integrated network system that combines an underwater network, a space network, and the traditional terrestrial mobile network to give ubiquitous network connectivity. The three primary communication technologies that enable underwater radio communications are acoustic, RF, and optical [52]. Even with all of the suggested technologies and solutions, underwater communication still requires improvement. The growing demand for wide-ranging applications, including pollution management, disaster forecasting, military operations, and environmental monitoring, has led to an upward trend in the number of research investigations on underwater WSNs [53]. NEPTUNE underwater acoustic networking in Canada and Seaweb underwater acoustic networking in the U.S. are two noteworthy applications [54], [55]. Through the use of an underwater acoustic communications network, the U.S. Office of Naval Research (ONR)-funded persistent littoral undersea surveillance network (PLUSNet) demonstrated multi-sensor and multi-vehicle anti-submarine warfare (ASW) [56]. However, a few of the primary obstacles to underwater sensor deployments include the propagation medium's severe attenuation, the acoustic wave's sluggish speed of propagation, and the sensor nodes' restricted energy supply [53]. Some research efforts, like [53], looked at clustering technologies to enhance communication performance and energy consumption. It is crucial to remember that the application, the surrounding environment, and the enabling technology should all be taken into account while adopting a clustering technique.

We discuss two perceived LoRaWAN applications [57], [58] in the following subsections.

A. LORAWAN APPLICATION-1: REMOTE UNCONNECTED AREAS FOR ENVIRONMENTAL MONITORING

LoRa transceivers were considered for sending data from sensors on the ground to High-Altitude Platform Stations (HAPs) for Remote unconnected areas for environmental monitoring applications [57]. According to the current research articles, to cover remote places that would not otherwise be able to access the Internet, 5G and 6G mobile communication systems will feature an NTN that will contain various satellite systems such as Low Earth Orbit (LEO) satellites and Geostationary (GEO) satellites, in addition to HAPs in the stratosphere. HAPs are defined by ITU Radio Regulations as radio stations situated on a flying object between 20 and 50 km in altitude and operating under the High altitude IMT Base Stations (HIBS). The authors in [57] considered aerostatic type HAPs out of the three kinds of HAPs: balloons, fixed-wing platforms, and airships. These HAPs use a control system to stay inside a cylinder with a 400 m radius and a height of around 700 m to mitigate the impact of severe winds in the stratosphere. The authors considered a LoRaWAN-based IoT system that can host a LoRA Gateway (GW) and uses HAPs to connect remote IoT devices to the Internet. The HAPs relays the received data using a communication link with the ground.

There are many path loss models for air-to-ground (A2G) and ground-to-air (G2A) communications in the literature. However, according to the authors of [57], the main problem was determining which model would work best in the 868 MHz Industrial, Scientific, and Medical (ISM) frequency band, particularly in a remote or rural area, and with HAPs at stratospheric altitude. The authors used the information available for transmissions at 2 GHz, 3.5 GHz, and 5.5 GHz to approximate some parameter values at 868 MHz. However, we would like to add that Semtech released the first LoRa module working at 2.4 GHz in 2017, even though the 2.4 GHz ISM spectrum is not yet part of the standard LoRaWAN frequency plans. In a recent article, the authors in [59] found that LoRaWAN at 2.4 GHz is a viable solution for scenarios characterized by a high density of nodes in a limited area, while the EU 868 MHz spectrum (Europe) remains the preferred choice for a larger area. Three LoRaWAN variants are compared in [60]: the ones that operate in the 2.4 GHz, US915, and EU868 ISM bands.

B. LORAWAN APPLICATION-2: REMOTE MONITORING OF OFFSHORE WIND FARMS

The possibility of using satellite and massive machine-type connectivity (mMTC) to enable remote monitoring of offshore wind farms was explored in [58]. Two-thirds of the electricity produced in the European Union (EU) from renewable sources came from wind and hydropower, while the total installed capacity of wind power producers worldwide surpasses 650.8 Gigawatt. Although they cost more to construct, offshore wind farms are more efficient than their onshore counterparts and are less susceptible to public disapproval. Through the construction of offshore

wind turbine farms and ambitious plans, Denmark, Norway, the United Kingdom, and the USA have demonstrated a remarkable interest in offshore wind electricity generation in recent years. Based on the available data, an offshore wind turbine needs five maintenance visits a year on average, and the total cost of repairs accounts for around 30% of the turbine's life-cycle expenses. By the third year of operation, an offshore wind turbine has an average failure rate of roughly ten failures per turbine annually, of which 80% are minor repairs, 17.5% are major repairs, and 2.5% are major replacements based on material cost.

Pre-emptive maintenance and sophisticated remote surveillance and monitoring systems have a great potential to prevent breakdowns, which would lower operating costs and shorten the amount of time the wind turbine is offline due to failure. Because of the low frequency of updates, conventional wind farm condition monitoring systems (CMSs) lack real-time monitoring and failure prediction capabilities. Instead, they consist of a complicated communication infrastructure with a specialized wired network running over a considerable distance. However, transferring the collected sensor data presents another difficulty in offshore wind farm monitoring, as well as monitoring in remote areas generally, due to the absence of the conventional communication infrastructure. According to the authors in [58], there are two main approaches that can be taken to address this difficulty. One approach is backbone connectivity through a satellite channel to the local GW. The alternative is putting new non-terrestrial infrastructures such as drones, high-altitude balloons, and satellites to provide connectivity in isolated places. WSN-based health tracking of the hub, tower, nacelle, and blades of offshore wind turbines is considered by many researchers. The authors in [58] considered two distinct architectural styles: direct and indirect. A local mMTC gateway (GW) with a backbone over a reliable communication channel, i.e., satellite or wire-based, is the foundation of the indirect architecture. In the direct approach, the mMTC GW on the LEO satellite receives the data directly from the wind turbine sensors. The mMTC (LoRaWAN) and satellite integration have been endorsed by the authors in [58] for wireless condition monitoring of large-dense offshore wind farms. However, we noted that there was no discussion on the system reliability requirements.

III. LORAWAN NODE DISTRIBUTION

In this section, we demonstrate that a uniform distribution does not support the optimal (full capacity and maximum coverage) LoRaWAN node distribution. Alternatively, by carefully selecting the mean and standard distribution, we can use the Gaussian distribution to satisfy the optimal distribution constraints. An alternative approach is presented as well. We also go over some pertinent research that has been done in the literature regarding node distribution in LoRa networks. However, unlike our work, they did not provide the comprehensive mathematical foundation needed to simulate a network that guarantees the optimal LoRaWAN node distribution scenarios.

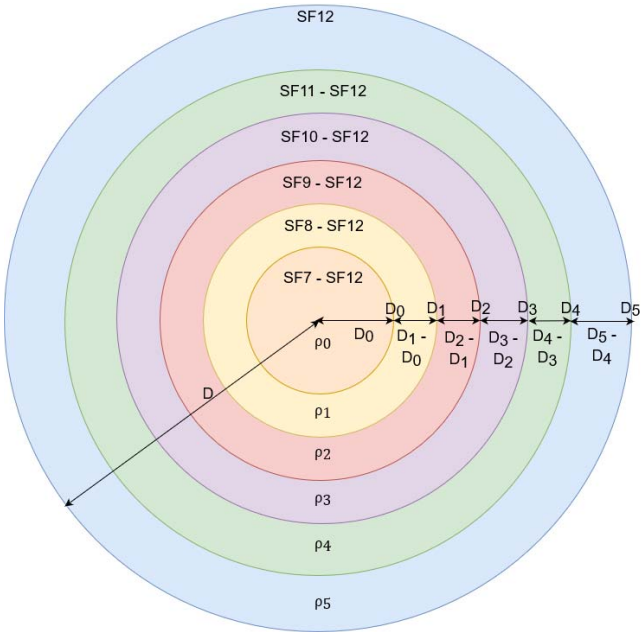

FIGURE 1. LoRaWAN node distributions.

To see the spread of LoRaWAN nodes with maximum network coverage D, we can consult Figure 1. The entire network can be divided into six distinct regions. Each region is unique in terms of the maximum number of nodes that can be supported, the number of nodes in a specific application, and the applicable data rates.

Before we can imitate such a network, we must first determine the constraints for the optimal LoRa node distribution situation. We perform the following actions:

1. First, we calculate D_i.
2. Next, we calculate $n_{DR(i)}$ associated with $SF(j)$.
3. After that, we determine the optimal LoRaWAN node distribution constraints.
4. Finally, following a trial and error method, we find an appropriate mean and standard distribution for Gaussian distribution to mimic optimal LoRaWAN node distribution.

A. FINDING D_I

This research uses the path loss model in [36], [38] to calculate the transmission coverage (d) in the manner described below.

$$d = 10^{\mathrm{PL}-23.3-21\log_{10}(f/900\ \mathrm{MHz})/37.6}, \tag{1}$$

where PL is the link budget, and f is the operating frequency.

One can compute the maximum link budget ($PL_{max_{SF(j)}}$) for a given SF as

$$PL_{max_{SF(j)}} = P_{tx_{max}} + rx_{sens_{SF(j)}}, \tag{2}$$

where $P_{tx_{max}}$ is the maximum transmit power, and $rx_{sens_{SF(j)}}$ is the receiver sensitivity associated with $SF(j)$.

Referring to Figure 1, D_i is the maximum transmission distance for $SF(i+7)$, which can be obtained as

$$D_i = 10^{\mathrm{PL}_{\max_{\mathrm{SF(i+7)}}} - 23.3 - 21\log_{10}(f/900\ \mathrm{MHz})/37.6}. \quad (3)$$

B. FINDING $N_{DR(I)}$ ASSOCIATED WITH SF(J)

ToA refers to the time required for the completion of packet transmission. ToA for LoRa channels and GFSK channels can be calculated as [13]

$$ToA_{LoRA} = \frac{2^{SF}}{BW}\Bigg((n_{premble} + 4.25) + \Bigg(SW + \max\Bigg(\Bigg(ceil\Bigg(\frac{8PL - 4SF + 28 + 16CRC - 20IH}{4(SF - 2DE)}\Bigg)(CR+4)\Bigg), 0\Bigg)\Bigg)\Bigg), \quad (4)$$

and

$$ToA_{GFSK} = \frac{8}{DR}\big(n_{preamble} + SW + PL + 2CRC\big), \quad (5)$$

where SF is the spreading factor and BW is the bandwidth. $n_{preamble}$ represents the number of preamble symbols in a LoRaWAN frame. For LoRa channels, $n_{preamble}$ is 8 bytes, and for GFSK channels, it is 5 bytes. Similarly, SW represents the length of the synchronization word, with 8 bits for LoRa channels and 3 bytes for GFSK channels. The cyclic redundancy check (CRC) is used to check the integrity of the payload. $IH = 1$ when implicit header mode is enabled, and $IH = 0$ when explicit header mode is enabled. DE is used for data rate optimization. $DE = 1$ for low data rate optimization, and $DE = 0$ for all other cases. CR represents the coding rate from 1 to 4. DR is the data rate, and $DR = 50$ kbps for the GFSK channels. Ceil represents the ceiling function.

In ALOHA, only 18.4% of successful transmission can be achieved during one frame time. Although the authors in [15] developed an expression to calculate the network capacity, some corrections are required.

Note that each $SF(j)$ supports a unique data rate ($DR(i)$). For example, DR0 represents LoRa: SF12/125 kHz. Since packet transmission in LoRaWAN is similar to ALOHA, the maximum number of nodes supported by a particular data rate ($n_{DR(i)}$ or $n_{SF(j)}$) is given by

$$n_{DR(i)} or n_{SF(j)} = \begin{cases} \left\lfloor \frac{0.5}{e \times n_a \times ToA_i} \right\rfloor \times l_{BW} \\ \text{or,} \\ \left\lfloor \frac{0.5 \times T_i}{e \times n_a \times L_{DP} \times 8} \right\rfloor \times l_{BW} \end{cases}, \quad (6)$$

where n_a is the node activity rate, l_{BW} is the number of channels, and L_{DP} is the packet size. T_i is the throughput associated the data rate $DR(i)$ and can be calculated as

$$T_i = \frac{L_{DP}}{ToA_i}. \quad (7)$$

C. OPTIMAL LORAWAN NODE DISTRIBUTION CONSTRAINTS

Let ρ_i be the number of nodes that fall between D_i and D_{i-1}. Nodes served by the network (ρ) can be calculated as

$$\rho = \sum_{i=0}^{5} \rho_i. \quad (8)$$

We can express $\rho_{i_{max}}$ as

$$\rho_{i_{max}} = n_{SF(i+7)} + \sum_{j=i+1}^{5} \big(\rho_{j_{max}} - \rho_j\big), \quad (9)$$

where $\rho_{5_{max}} = n_{SF12}$.

Let n_i be the number of nodes within distance D_i. Then, we can express $n_{i_{max}}$ as

$$n_{i_{max}} = \rho_{max} - \sum_{j=i+1}^{5} \rho_j, \quad (10)$$

where $\rho_{max} = \sum_{j=7}^{12} n_{SF(j)}$.

$\rho_{i_{max}}$ and $n_{i_{max}}$ set the constraints for optimal LoRaWAN node distributions.

D. GENERATING A LORA NETWORK WITHOUT VIOLATING OPTIMAL NODE DISTRIBUTION CONSTRAINTS USING GAUSSIAN DISTRIBUTION

For full-capacity LoRa networks ($\rho = \rho_{max}$), we need to achieve the following condition to be able to use the uniform distribution.

$$\frac{D_i - D_{i-1}}{\rho_i} = \frac{D_{i+1} - D_i}{\rho_{i+1}}, i = [0, 5]. \quad (11)$$

Since it is not possible to achieve the above condition, we conclude that the uniform distribution can not be used for full-capacity LoRa networks. Interested readers can verify it using the formulas presented in Sections III-A, III-B, and III-C.

Next, we explore the Gaussian distribution. A Gaussian distribution is described by $f(x) = \frac{1}{\sigma\sqrt{2\pi}} e^{-\frac{1}{2}(\frac{x-\mu}{\sigma})^2}$, where μ is the mean of the distribution and σ is its standard deviation. Different values of μ and σ will yield different normal distributions. An appropriate choice of the parameter values can be achieved by trial and error.

Wireless technologies are limited in their capacity to optimize specific parameters, such as channel bandwidth, scalability, battery lifetime, data rate, operational frequency band, and feasible range [61]. To evaluate LoRaWAN, we considered the SX1272 transceiver [62] and the path loss model from [36], [38], for which the maximum attainable transmission range is approximately 3.7 km. Table 1 represents the optimal node distribution in LoRaWAN when five 125 KHz LoRa channels and one 250 KHz LoRa channel are used with 8-bytes packet and 0.1/s message transaction rate. We observed that only about 75 out of 767 nodes could reside outside 2.39 km. The percentage distribution can vary slightly depending on various factors

TABLE 1. Optimal node distribution in LoRaWAN for 8 bytes packet, message transaction rate 0.1 and 5 125-kHz-LoRa-channels/1 250-kHz-LoRa- channel.

Distance from GW (km)	Percentage of Nodes
1.66	56.73
1.99	76.96
2.39	89.27
2.87	95.41
3.25	98.46

TABLE 2. Node distribution pattern generated by Gaussian distribution with mean 0 and standard deviation 1.2.

Distance from GW (km)	Percentage of Nodes
0.9175	45.30
1.835	89.10
2.7525	99.10
3.67	100

Algorithm 1 Generate a LoRa Network Without Violating Optimal Node Distribution Constraints

Data: $[D_i]$, ρ_{max}
Result: $z = []$
Define: $\rho_{i_{max}}, n_{i_{max}}$
$D_{max} \leftarrow D_5$
while $i \leq \rho_{max}$ **do** $z \leftarrow g_2(g_1(D_{max}), \rho_{i_{max}}, n_{i_{max}})$
if $g_2(g_1(D_{max}), \rho_{i_{max}}, n_{i_{max}}) \neq -1$ **then** $i = i + 1$;
end if
end while

such as channel combinations, message transaction rate, and packet size. Nevertheless, only a small fraction of nodes can be supported by higher SFs. We used the trial and error method to find a suitable value of μ and σ, where we set μ and $\sigma \in [0, 2]$. As an example, the node distribution scenario presented in Table 2 was generated using a Gaussian distribution with mean and standard deviation values of 0 and 1.2, respectively, without violating node distribution constraints.

E. AN ALTERNATIVE APPROACH TO GENERATE A LORA NETWORK WITHOUT VIOLATING OPTIMAL NODE DISTRIBUTION CONSTRAINTS

In Section III-D, we showed that it is possible to generate a LoRa network without violating optimal node distribution constraints using a Gaussian distribution, where μ and σ were chosen using a trial and error method. We can, however, generate the node distribution for optimal LoRa network using Algorithm 1.

In Algorithm 1, $[D_i]$ contains the values of D_i, D_{max} is the maximum network coverage, and $\rho_{max} = \sum_{j=7}^{12} n_{SF(j)}$. Expressions (9) and (10) are used to define $\rho_{i_{max}}$ and $n_{i_{max}}$. g_1 generates a random point inside the network coverage D_{max}. g_2 keeps track of the values of ρ_i and n_i. If an iteration violates the conditions for $\rho_{i_{max}}$ or $n_{i_{max}}$, g_2 returns -1. Otherwise, a node location is assigned to z, and the counter i is incremented by 1.

LoRaWAN capacity was analyzed in [13], [63]. The authors in [13] found that for network coverage of 8.92 km, less than 10% of nodes can reside at a distance over 5 km from the GW. Their findings suggest that 73% of nodes must reside within 3.31 km when three 125 KHz LoRa channel are used, and 87% of nodes have to reside within 3.31 km when three 125 KHz LoRa channels and one GFSK channel are used. The authors in [63] claimed that peak system coverage and capacity require 76% of end nodes confinement within 26% of the peak coverage area while support is provided to only 1% of nodes by the highest data rate. Apart from offering appropriate node distribution constraints, we did, however, rectify the formula for capacity. We also demonstrate the use of a Gaussian distribution and an alternative approach to generate an optimal LoRa network.

IV. ROLES OF CLUSTER FORMATION ON ENERGY CONSUMPTION IN MULTI-HOP ROUTING

Successful packet delivery can be improved for each end node by using relay nodes under conditions where direct communication between an end node and the GW is impossible [39]. The feasibility of concurrent transmissions in multi-hop LoRa networks has been demonstrated in [40]. Nevertheless, multi-hop routing is more energy-efficient than single-hop routing [38]. Our developed Extended-DRESG scheme in [47] divides the nodes in the network into different clusters by placing virtual rings around the GW following a distance spreading model, and clustering is achieved with the node-ring association in which a node is assigned to its closest ring. Depending on the number of clusters/virtual rings (R), $R!$ ring-hop combinations are possible. The child-parent relationship matrix establishes node-to-node association among the clusters for packet forwarding in different ring-hop combinations. The optimal ring-hop combination is the one for which critical nodes consume the least energy among all possible ring-hop combinations and are obtained through simulations. The child-parent-relationship matrix tells us about the number of packets forwarded by a node in a given ring.

We will explore the scheme in detail with $R = 3$ to identify the role of different variables and, therefore, the insights for performance improvement.

Possible ring-hop combinations for $R = 3$ can be obtained from Table 3 [47]. The total energy ($e^{[\text{tot}]}(r)$) consumed by a representative node given a ring r can be calculated as

$$e^{[\text{tot}]}(r) = e^{[\text{tx}]}(r) + e^{[\text{rx}]}(r), \tag{12}$$

where $e^{[\text{tx}]}(r)$ and $e^{[\text{tx}]}(r)$ are the packet transmission and reception energy, respectively.

The connectivity matrix (Λ) represents the ring-hop-combinations and can be generated from Table 3 as [47]

$$\Lambda_1 = \begin{bmatrix} 1 & 1 & 1 \\ 0 & 1 & 1 \\ 0 & 0 & 1 \end{bmatrix}, \quad \Lambda_2 = \begin{bmatrix} 1 & 1 & 1 \\ 0 & 1 & 0 \\ 0 & 0 & 1 \end{bmatrix},$$

TABLE 3. Ring-hop combinations for $R = 3$.

Ring-hop combination	# of hops for ring 1	# of hops for ring 2	# of hops for ring 3
1 (NRH)	1	1	1
2 (VH)	1	1	2
3 (VH)	1	1	3
4 (VH)	1	2	1
5 (VH)	1	2	2
6 (DH)	1	2	3

$$\Lambda_3 = \begin{bmatrix} 1 & 1 & 0 \\ 0 & 1 & 0 \\ 0 & 0 & 1 \end{bmatrix}, \quad \Lambda_4 = \begin{bmatrix} 1 & 0 & 0 \\ 0 & 1 & 1 \\ 0 & 0 & 1 \end{bmatrix},$$
$$\Lambda_5 = \begin{bmatrix} 1 & 0 & 1 \\ 0 & 1 & 0 \\ 0 & 0 & 1 \end{bmatrix}, \quad \Lambda_6 = \begin{bmatrix} 1 & 0 & 0 \\ 0 & 1 & 0 \\ 0 & 0 & 1 \end{bmatrix},$$

where Λ_1 represents Next-Ring-Hop (NRH) routing, where nodes in a ring can communicate with the nodes in the ring immediately below it, while only the nodes in the first ring can communicate with the GW. Λ_6 represents Direct-Hop (DH) routing or single-hop routing where nodes communicate with the GW directly. Other matrices represent different Variable-Hop (VH) routings or ring-hop combinations for the nodes to reach the GW. $\Lambda_{i,j} = 1$ represents the i-th ring forwards the packets from the j-th ring.

The child-parent relationship matrix (c), according to the multi-hop routing scheme presented in [47], can be represented as

$$C_1 = \begin{bmatrix} 0 & 0 & 0 \\ x_1 & 0 & 0 \\ 0 & x_2 & 0 \end{bmatrix}, \quad C_2 = \begin{bmatrix} 0 & 0 & 0 \\ x_1 & 0 & 0 \\ x_3 & 0 & 0 \end{bmatrix},$$
$$C_3 = \begin{bmatrix} 0 & 0 & 0 \\ x_1 & 0 & 0 \\ 0 & 0 & 0 \end{bmatrix}, \quad C_4 = \begin{bmatrix} 0 & 0 & 0 \\ 0 & 0 & 0 \\ 0 & x_2 & 0 \end{bmatrix},$$
$$C_5 = \begin{bmatrix} 0 & 0 & 0 \\ 0 & 0 & 0 \\ x_3 & 0 & 0 \end{bmatrix}, \quad C_6 = \begin{bmatrix} 0 & 0 & 0 \\ 0 & 0 & 0 \\ 0 & 0 & 0 \end{bmatrix},$$

where $C_{j,i}$-refers to the number of packets from the j-th ring forwarded by a node in the i-th ring. For the above example scenario with $R = 3$, C_1 represents the child-parent relationship matrix for NRH where $C_{1_{2,1}} = x_1$ represents the number of packets sent by a node in ring-2 to ring-1.

The transmit, receive, and total energy consumptions of the representative nodes in different rings can be calculated as follows.

Ring-hop combinations-1: In this combination, nodes in the first ring are typically the critical nodes, and thus, the energy consumption of those nodes is calculated only as

$$e_c^{[\mathrm{tx}]} = (1 + x_1 + x_1x_2) \times \frac{L_{\mathrm{DP}}}{s^{[\mathrm{tx}]}} \times I_1^{[\mathrm{tx}]}(p) \times V_{\mathrm{DD}}, \quad (13)$$

and

$$e_c^{[\mathrm{rx}]} = (x_1 + x_1x_2) \times \frac{L_{\mathrm{DP}}}{s^{[\mathrm{tx}]}} \times I^{[\mathrm{rx}]} \times V_{\mathrm{DD}}, \quad (14)$$

where $e_c^{[\mathrm{tx}]}$ and $e_c^{[\mathrm{rx}]}$ are the critical nodes' transmit and receive energies, respectively. $x_i \in \mathbb{Z}^+$, L_{DP} is the packet size, $s^{[\mathrm{tx}]}$ and $I_1^{[\mathrm{tx}]}$ are the data rate and transmission current associated with a particular transmit power, respectively, V_{DD} is the operating voltage, and $I^{[\mathrm{rx}]}$ is the reception current.

Similarly, we obtain the energy consumption expressions for other ring-hop combinations, as shown below. Please note that $I_2^{[\mathrm{tx}]}$, $I_3^{[\mathrm{tx}]}$, $I_4^{[\mathrm{tx}]}$ and $I_5^{[\mathrm{tx}]}$ represent current consumption associated with different transmit power levels.

Ring-hop combinations-2:

$$e^{[\mathrm{tx}]}(r = 1) = (1 + x_1 + x_3) \times \frac{L_{\mathrm{DP}}}{s^{[\mathrm{tx}]}} \times I_1^{[\mathrm{tx}]}(p) \times V_{\mathrm{DD}}, \quad (15)$$
$$e^{[\mathrm{rx}]}(r = 1) = (x_1 + x_3) \times \frac{L_{\mathrm{DP}}}{s^{[\mathrm{tx}]}} \times I^{[\mathrm{rx}]} \times V_{\mathrm{DD}}, \quad (16)$$
$$e^{[\mathrm{tx}]}(r = 2) = \frac{L_{\mathrm{DP}}}{s^{[\mathrm{tx}]}} \times I_2^{[\mathrm{tx}]}(p) \times V_{\mathrm{DD}}, \quad (17)$$
$$e^{[\mathrm{rx}]}(r = 2) = 0, \quad (18)$$
$$e^{[\mathrm{tx}]}(r = 3) = \frac{L_{\mathrm{DP}}}{s^{[\mathrm{tx}]}} \times I_3^{[\mathrm{tx}]}(p) \times V_{\mathrm{DD}}, \quad (19)$$

and

$$e^{[\mathrm{rx}]}(r = 3) = 0. \quad (20)$$

Ring-hop combinations-3:

$$e^{[\mathrm{tx}]}(r = 1) = (1 + x_1) \times \frac{L_{\mathrm{DP}}}{s^{[\mathrm{tx}]}} \times I_1^{[\mathrm{tx}]}(p) \times V_{\mathrm{DD}}, \quad (21)$$
$$e^{[\mathrm{rx}]}(r = 1) = x_1 \times \frac{L_{\mathrm{DP}}}{s^{[\mathrm{tx}]}} \times I^{[\mathrm{rx}]} \times V_{\mathrm{DD}}, \quad (22)$$
$$e^{[\mathrm{tx}]}(r = 2) = \frac{L_{\mathrm{DP}}}{s^{[\mathrm{tx}]}} \times I_2^{[\mathrm{tx}]}(p) \times V_{\mathrm{DD}}, \quad (23)$$
$$e^{[\mathrm{rx}]}(r = 2) = 0, \quad (24)$$
$$e^{[\mathrm{tx}]}(r = 3) = \frac{L_{\mathrm{DP}}}{s^{[\mathrm{tx}]}} \times I_4^{[\mathrm{tx}]}(p) \times V_{\mathrm{DD}}, \quad (25)$$

and

$$e^{[\mathrm{rx}]}(r = 3) = 0. \quad (26)$$

Ring-hop combinations-4:

$$e^{[\mathrm{tx}]}(r = 1) = \frac{L_{\mathrm{DP}}}{s^{[\mathrm{tx}]}} \times I_1^{[\mathrm{tx}]}(p) \times V_{\mathrm{DD}}, \quad (27)$$
$$e^{[\mathrm{rx}]}(r = 1) = 0, \quad (28)$$
$$e^{[\mathrm{tx}]}(r = 2) = (1 + x_2)\frac{L_{\mathrm{DP}}}{s^{[\mathrm{tx}]}} \times I_5^{[\mathrm{tx}]}(p) \times V_{\mathrm{DD}}, \quad (29)$$
$$e^{[\mathrm{rx}]}(r = 2) = x_2 \times \frac{L_{\mathrm{DP}}}{s^{[\mathrm{tx}]}} \times I^{[\mathrm{rx}]} \times V_{\mathrm{DD}}, \quad (30)$$
$$e^{[\mathrm{tx}]}(r = 3) = \frac{L_{\mathrm{DP}}}{s^{[\mathrm{tx}]}} \times I_6^{[\mathrm{tx}]}(p) \times V_{\mathrm{DD}}, \quad (31)$$

and

$$e^{[\mathrm{rx}]}(r = 3) = 0. \quad (32)$$

Ring-hop combinations-5:

$$e^{[\mathrm{tx}]}(r=1) = (1+x_3) \times \frac{L_{\mathrm{DP}}}{s^{[\mathrm{tx}]}} \times I_1^{[\mathrm{tx}]}(p) \times V_{\mathrm{DD}}, \quad (33)$$

$$e^{[\mathrm{rx}]}(r=1) = x_3 \times \frac{L_{\mathrm{DP}}}{s^{[\mathrm{tx}]}} \times I^{[\mathrm{rx}]} \times V_{\mathrm{DD}}, \quad (34)$$

$$e^{[\mathrm{tx}]}(r=2) = \frac{L_{\mathrm{DP}}}{s^{[\mathrm{tx}]}} \times I_5^{[\mathrm{tx}]}(p) \times V_{\mathrm{DD}}, \quad (35)$$

$$e^{[\mathrm{rx}]}(r=2) = 0, \quad (36)$$

$$e^{[\mathrm{tx}]}(r=3) = \frac{L_{\mathrm{DP}}}{s^{[\mathrm{tx}]}} \times I_3^{[\mathrm{tx}]}(p) \times V_{\mathrm{DD}}, \quad (37)$$

and

$$e^{[\mathrm{rx}]}(r=3) = 0. \quad (38)$$

Ring-hop combinations-6: Since this ring-hop combination represents single-hop or Direct-Hop (DH) routing, the furthest nodes from the GW are the critical nodes, and thus, the energy consumption of the critical nodes can be obtained as

$$e_c^{[\mathrm{tx}]} = \frac{L_{\mathrm{DP}}}{s^{[\mathrm{tx}]}} \times I_4^{[\mathrm{tx}]}(p) \times V_{\mathrm{DD}}, \quad (39)$$

and

$$e_c^{[\mathrm{rx}]} = 0. \quad (40)$$

Based on ring positions and hop counts, we can also write in general

$$I_1 < I_3 < I_4, \quad (41)$$

$$I_2 \leq I_1, \quad (42)$$

$$I_6 \leq I_1, \quad (43)$$

and

$$I_5 \simeq I_3. \quad (44)$$

The energy consumption of the critical nodes ($e_c^{[\mathrm{tot}]}$) can be found as

$$e_c^{[\mathrm{tot}]} = \max((e^{[\mathrm{tx}]}(r=1) + e^{[\mathrm{rx}]}(r=1)), (e^{[\mathrm{tx}]}(r=2) + e^{[\mathrm{rx}]}(r=2)), (e^{[\mathrm{tx}]}(r=3) + e^{[\mathrm{rx}]}(r=3))). \quad (45)$$

The above expression can be generalized for any number of virtual rings as,

$$e_c^{[\mathrm{tot}]} = \max_{r=1,2\cdots R} \left(e^{[\mathrm{tx}]}(r) + e^{[\mathrm{rx}]}(r)\right). \quad (46)$$

Transmit current is directly related to the transmit power used by an end node in achieving the required link budget to meet transmission distance. Therefore, the node's location in the network and ring-hop combinations determine the minimum transmit power requirement for an end node. The operating voltage (V_{DD}) is 3V. For typical applications, packet size (L_{DP}) is fixed, and the data rate ($s^{[\mathrm{tx}]}$) depends on the bandwidth/SF combination. From the expressions developed for the six ring-hop combinations, for the example case of $R = 3$, it can be seen that the number of relaying packets in each ring plays a critical role in the energy consumption of critical nodes. The best ring-hop combination is one of the above six combinations for which the critical nodes' energy consumption is minimal.

Algorithm 2 Generate Matrix K

```
Data: Λ
Result: K
K ← Λ
for i = 1:(R − r) do
    if Λ_{r,r+i} = 1 then
        for j = r + 1:R do
            if Λ_{j,r+i} = 0 then K_{j,r+i} = 1
            else K_{j,r+i} = C_{j,r+i−h_j}
            end if
        end for
    end if
end for
```

V. PROPOSED METHOD FOR FINDING OPTIMAL RING POSITIONING AND RING-HOP COMBINATION

The extended-DRESG routing scheme offers optimized energy consumption of critical nodes by deciding on the optimal ring-hop-combination for a given number of rings, which were positioned following some ring-spreading models. However, the impact of ring positions was unclear, and thus, possibilities of further improvement remained an open research topic. In this section, we provide the solution to find the optimal ring-positions and ring-hop-combination that optimizes the energy consumption of critical nodes.

Expression (12) can be written as

$$e^{[\mathrm{tot}]}(r) = \frac{L_{\mathrm{DP}}}{s^{[\mathrm{tx}]}} \times V_{\mathrm{DD}} \times \left\{(1+x(r)) \times I^{[\mathrm{tx}]}(r) + x(r) \times I^{[\mathrm{rx}]}\right\}, \quad (47)$$

where $x(r)$ is the number of packets received by ring r from other rings.

Let $m = \frac{D}{a}$ be the number of equally spaced rings, where D is the maximum wireless coverage. For R rings, the optimal ring positions and the ring-hop combination is one of the $\binom{m-1}{R-1} \times R!$ combinations. When a is small, sufficient points in the space of interest can be guaranteed. Observations from expressions (46) and (47) suggest that the desired ring positions and ring-hop combinations is the one for which ($e_c^{[\mathrm{tot}]}$) is minimum corresponding to the minimum $x(r_c) \times I^{[\mathrm{tx}]}(r_c)$.

A. DETERMINING X(R)

For R rings designated as $r_1, r_2, \ldots, r_R$ and hop numbers $h_1, h_2, \ldots, h_R$, $x(r)$ can be written as

$$x(r) = \sum_{j=r+1}^{R} \prod_{i=r}^{R} K_{i,j}, \quad (48)$$

where matrix K can be obtained from connectivity matrix (Λ) and Child-Parent-Relationship matrix (C) following Algorithm 2.

Let λ be the diagonal matrix. The connectivity matrix Λ can be obtained following Algorithm 3.

Algorithm 3 Generate Connectivity Matrix Λ

```
Data: h = h_1, h_2, ...., h_R
Result: Λ
Λ ← λ
for i = R:2 do
    for j = 1:R do
        if Λ_{i,j} = 1 then Λ_{i−h_j,j} = 1
        end if
    end for
end for
```

B. DETERMINING $I^{[TX]}(R)$

For R rings with radius $d_1, d_2, \ldots, d_R$ and hop numbers $h_1, h_2, \ldots, h_R$, packet forwarding distances ($d_f = \{d_{f_1}, d_{f_2}, \ldots, d_{f_R}\}$) for the rings can be found by,

$$d_{f_r} = d_r - d_{r-h_r}, \tag{49}$$

where the GW is located at $(0, 0)$ and $d_0 = 0$. For R rings, $d_R = D$ to ensure full network coverage and $P = \{d_1, d_2, \ldots, d_{R-1}\} \subset Q = \{a_1, a_2, \ldots, .., a_{m-1}\}$, where $a_1 = a$, $a_2 = 2a$ and $a_{m-1} = (m-1)a$. The minimum link budgets ($PL(d_{f_1}), PL(d_{f_2}), \ldots, PL(d_{f_R})$) required for d_f can be found by utilizing expression (5). The required transmit power $P_{tx}(r)$ can be found by

$$P_{tx}(r) = PL\big(d_{f_r}\big) - rx_{sens}, \tag{50}$$

where rx_{sens} is the receiver sensitivity. Since rx_{sens} varies with the SFs, and the nodes can arbitrarily choose any of the available SFs, $P_{tx}(r)$ can be selected from $T = \{P_{tx}{:}P_{tx} \geq PL(d_{f_r}) - rx_{sens}\}$. In this article, the nodes choose the transmit power that ensures minimum energy consumption while satisfying the link budget requirements. Therefore we need to find $(P_{tx}(r) = \{P_{tx} \in T{:}P_{tx} \hat{=} I^{[\text{tx}]}, s^{[\text{tx}]} \implies e = \min\{\frac{L_{\text{DP}}}{s^{[\text{tx}]}} \times I^{[\text{tx}]} \times V_{\text{DD}}\}\})$.

C. DETERMINING OPTIMAL RING POSITIONS AND RING-HOP-COMBINATIONS

For R rings, let ring positions $d_o = \{d_{o_1}, d_{o_2}, \ldots, .., d_{o_R}\}$ and hop numbers $h_o = \{h_{o_1}, h_{o_2}, \ldots, .., h_{o_R}\}$ provide the optimal ring positions and ring-hop combination, which minimizes the energy consumption of critical nodes in the network.

For n nodes in the network, let $M_n = f_1(.)$ be a $n \times 2$ matrix that contains node co-ordinates, where $f_1(.)$ is the node distribution.

Let M_d be an $\binom{m-1}{r-1} \times R$ matrix, where $M_d(i, :)$ represents the r ring positions for the i-th combination. $M_d(i, r)$ is the radius of ring r in the combination i.

$M_d(i, :)$ corresponds to $R!$ ring-hop-combinations. The $R!$ ring-hop-combinations constitute the matrix M_H, where M_H is an $R! \times R$ matrix. $M_H(i, r)$ represents the hop counts for ring r in the ring-hop-combination i.

M_Λ is an $R! \times 1$ matrix, where the connectivity matrix Λ_i corresponds to $M_H(i, :)$.

M_K is an $R! \times R$ matrix where $M_K(i, r)$ represents the K Matrix for ring r in the ring-hop-combination i.

C is an $R \times R$ child-parent-relationship matrix where $C_{i,j}$ represents the child-parent-ratio between rings i and j. $C_{i,j} = \lceil \frac{n_i}{n_j} \rceil$, where n_i and n_j are the numbers of nodes in ring i and j and

$$C = f_1(M_n, M_r(i, :), r), \tag{51}$$

M_{d_f} is an $R! \times R$ matrix, where $M_{d_f(j,r)}$ represents the forwarding distance from ring r in ring-hop-combination j and

$$M_{d_f} = f_2(M_r(i, :), M_H), \tag{52}$$

M_I is an $R! \times R$ matrix, where $M_I(i, r)$ represents the required transmit current from ring r in ring-hop-combination i.

$$M_I = f_3\big(M_{d_f}, M_{TX}\big), \tag{53}$$

M_X is an $R! \times R$ matrix, where $M_X(i, r)$ represents the number of received packets by a node in ring r in ring-hop-combination i and

$$M_X = f_4(M_K, C), \tag{54}$$

M_E is an $R! \times R$ matrix, where

$$M_E = f_5(M_I, M_X), \tag{55}$$

and

$$M_E(i, j) = M_I(i, j) \times M_X(i, j). \tag{56}$$

M_S is an $R! \times 1$ matrix, where

$$M_S = f_6(M_E), \tag{57}$$

and

$$M_S(i) = max(M_E(i, :)). \tag{58}$$

M_C is an $\binom{m-1}{r-1} \times 2$ matrix, where

$$\begin{aligned} [M, I] &= min(M_S), \\ M_C(i, 1) &= M, \\ M_C(i, 2) &= I. \end{aligned} \tag{59}$$

M is the minimum value of M_S, and I represents the ring-hop-combination for which M_S is minimum.

Let,

$$[M_o, I_o] = min(M_C(:, 1), \tag{60}$$

and

$$T = M_C(I_o, 2). \tag{61}$$

Then, the optimal ring positions and hop numbers can be found as

$$d_o = M_d(I_o, :), \tag{62}$$

and,

$$h_o = M_H(T, :). \tag{63}$$

The optimal ring positions and the ring-hop combination can be obtained following Algorithm 4.

Algorithm 4 Finding the Optimal Ring Positions and Ring-Hop Combinations

Data: D, a, R
Result: d_o, h_o
$m \leftarrow \frac{D}{a}$
$M_n \leftarrow f_1(.)$
$M_d \leftarrow f_2(m, R)$
$M_H \leftarrow f_3(R)$
$M_\Lambda \leftarrow f_4(R, M_H)$
$M_{TX} \leftarrow f_5(.)$
while $i = 1{:}\binom{m-1}{R-1}$ **do**
  $C \leftarrow f_6(M_n, M_d(i, :), R)$
  $M_K \leftarrow f_7(M_\Lambda, C, R)$
  $M_{d_f} \leftarrow f_8(M_d(i, :), M_H)$
  $M_I \leftarrow f_9(M_{d_f}, M_{TX})$
  $M_X \leftarrow f_{10}(M_K, R)$
  $M_E \leftarrow f_{11}(M_I, M_X)$
  $M_S \leftarrow f_{12}(M_E)$
  $M_C \leftarrow f_{13}(M_S)$
end while
$[M_0, I_0] \leftarrow min(M_C(:, 1))$
$T \leftarrow M_C(I_0, 2)$
$d_o = M_d(I_0, :)$
$h_o = M_H(T, :)$

D. TIME COMPLEXITY

Finding the optimal ring positions and ring-hop combinations has a time complexity of $O(n + km^{R-1})$, where n is the number of nodes. $m = \frac{D}{a}$, where D is the network coverage in kilometers and $a \approx 0$ (typically 0.001/0.0001). Lower values of a ensures more precise results when determining the optimal ring locations. While large values of R are theoretically feasible, 2, 3, 4, and 5 are the usual values of R. $k = \frac{1}{(R-1)!}((R-1)R!^2 + R^3R!)$. Note that, the algorithm is meant to be used offline, not online.

VI. PROPOSED CLUSTER FORMATION SCHEME

Based on the developed insights from the previous section, we propose an alternative way of implementing clusters for uniform node distribution. Instead of evaluating all possible ring positions, we can ensure $C_{j,i} \leq 1$ before evaluating $R!$ ring-hop combinations for which $e_c^{[\text{tot}]}$ is minimum. Therefore, a sufficient number of nodes are required in the lower rings than the upper rings, which allows for one-to-one node assignment. Below, we provide a cluster formation approach through which we can obtain our desired packet forwarding structure for uniform node distribution.

Consider a circular network coverage with the GW at the center and R cluster formations are required. Information about n end nodes locations is collected, and a database is created consisting of node-to-GW distances in ascending order. A virtual ring is an imagined ring that isolates a group of nodes from other nodes and, in association with other rings, assigns a cluster identity to that group of nodes. In this proposed method, starting with $i = 1$, the position of any i-th virtual ring is determined by considering the $(i * n/R)$-th database entry as the ring radius. The ceiling value of $(i*n/R)$ is used whenever the ratio turns out to be a fractional number. R clusters of nodes are formed following the inclusion of nodes in a cluster that falls in between any two consecutive rings, while the first cluster includes n/R nodes associated with the first n/R database entries. When n/R is an integer, all the clusters have an equal number of nodes, n/R.

Following the cluster formation technique proposed in this paper, the cluster-to-cluster relationship matrix for the example case of 3 clusters can be expressed as,

$$\mathbf{C} = \begin{bmatrix} 0 & 0 & 0 \\ 1 & 0 & 0 \\ 1 & 1 & 0 \end{bmatrix}$$

A one-to-one relationship can thus be established between any two clusters of nodes.

Let us find the child-parent relationship matrix and energy consumptions of nodes for ring-hop combination-2 for $R = 3$ rings in the example provided in the last section.

$$\mathbf{C}_2 = \begin{bmatrix} 0 & 0 & 0 \\ 1 & 0 & 0 \\ 1 & 0 & 0 \end{bmatrix}$$

Ring-hop combinations-2:

$$e^{[\text{tx}]}(r = 1) = 3 \times \frac{L_{\text{DP}}}{s^{[\text{tx}]}} \times I_1^{[\text{tx}]}(p) \times V_{\text{DD}}, \quad (64)$$

$$e^{[\text{rx}]}(r = 1) = 2 \times \frac{L_{\text{DP}}}{s^{[\text{tx}]}} \times I^{[\text{rx}]} \times V_{\text{DD}}, \quad (65)$$

$$e^{[\text{tx}]}(r = 2) = \frac{L_{\text{DP}}}{s^{[\text{tx}]}} \times I_2^{[\text{tx}]}(p) \times V_{\text{DD}}, \quad (66)$$

$$e^{[\text{rx}]}(r = 2) = 0, \quad (67)$$

$$e^{[\text{tx}]}(r = 3) = \frac{L_{\text{DP}}}{s^{[\text{tx}]}} \times I_3^{[\text{tx}]}(p) \times V_{\text{DD}}, \quad (68)$$

and

$$e^{[\text{rx}]}(r = 3) = 0. \quad (69)$$

The proposed cluster formation technique is based on the analysis developed in the previous section. It ensures that the number of relayed packets is reduced for the representative nodes in different rings. A one-to-one relationship between any two nodes from any two clusters for packet forwarding makes it possible. This goal can only be realized if the subsequent clusters have fewer nodes. The packet forwarding structures for different ring-hop combinations can be realized through observation of child-parent-relationship-matrix. Three different scenarios are presented in Figures 2, 3, and 4.

A. TIME COMPLEXITY

The proposed cluster formation and finding the optimal ring-hop combinations has a time complexity of $O(n + ((R-1)R!^2 + R^3R!))$, where n is the number of nodes, and R is the number of rings (typically, $R \leq 5$).

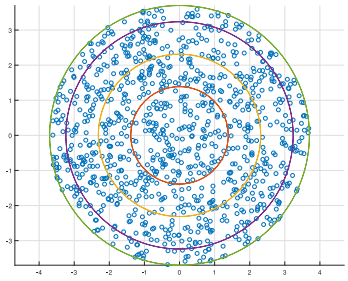

	Ring-1	Ring-2	Ring-3	Ring-4
Distance from the GW (km)	1.39	2.31	3.24	3.7

	In Ring-1	Between Ring-1 & Ring-2	Between Ring-2 & Ring-3	Between Ring-3 & Ring-4
Number of Nodes	153	261	375	211

Child-parent-relationship-matrix:

0 0 0 0
2 0 0 0
3 2 0 0
2 1 1 0

FIGURE 2. Packet forwarding structure in extended-DRESG with four virtual rings for 1000 uniformly distributed nodes.

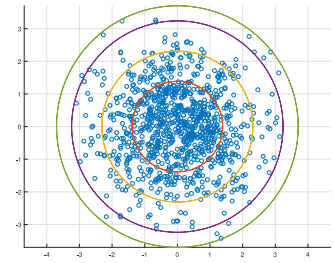

	Ring-1	Ring-2	Ring-3	Ring-4
Distance from the GW (km)	1.39	2.31	3.24	3.7

	In Ring-1	Between Ring-1 & Ring-2	Between Ring-2 & Ring-3	Between Ring-3 & Ring-4
Number of Nodes	507	351	126	16

Child-parent-relationship-matrix:

0 0 0 0
1 0 0 0
1 1 0 0
1 1 1 0

FIGURE 3. Packet forwarding structure in extended-DRESG with four virtual rings for 1000 gaussian distributed nodes.

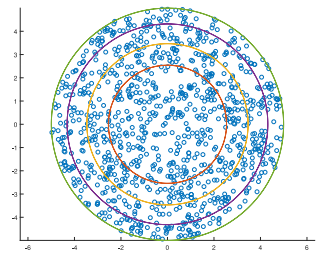

	Ring-1	Ring-2	Ring-3	Ring-4
Distance from the GW (km)	1.86	2.54	3.17	3.7

	In Ring-1	Between Ring-1 & Ring-2	Between Ring-2 & Ring-3	Between Ring-3 & Ring-4
Number of Nodes	250	250	250	250

Child-parent-relationship-matrix:

0 0 0 0
1 0 0 0
1 1 0 0
1 1 1 0

FIGURE 4. Packet forwarding structure in extended-DRESG with four virtual rings for 1000 uniformly distributed nodes following the new cluster formation scheme.

VII. SINGLE-HOP ROUTING AND NODE DISTRIBUTION

Multi-hop optimization is not achievable when all nodes are placed closely to the GW [4], as is the case in [64]. Network scalability was addressed in [64] through SF allocation while considering the coverage radius to be small enough that a transmission from a device configured with any SF can reach the GW. Referring to Figure 1, the advantages of multi-hop routing decrease with decreasing coverage area and vanish when the coverage radius changes from D_5 to D_0. Nevertheless, it is not an ideal scenario and contradicts one of the primary benefits of LoRa networks—wide coverage. Note that D_0 represents 50.76% of the maximum network coverage ($\approx$ 3.67 km) for the considered transceiver and path loss model in this paper. The values of D_0 and D_5 can be easily found by utilizing the SF7/125 KHz-LoRa-channel and SF12/125 KHz-LoRa-channel combinations, respectively.

In this study, we have emphasized other researchers' views as well as our own about the advantages of multi-hop routing over single-hop routing for LoRaWAN. In conclusion, multi-hop routing may be employed to increase energy efficiency or in situations when maintaining network connectivity proves to be difficult. However, due to its ease of usage, single-hop routing is still favoured for LoRaWAN. However, we recommend constructing the LoRaWAN node distribution in accordance with Section II for every routing when the maximum coverage and full capacity need to be taken into consideration. Other than the approach presented in this paper, we are not aware of any other approaches that will generate node distributions complying with the criteria for a LoRa network with maximum coverage and full capacity.

TABLE 4. Simulation parameters.

Number of Nodes	1,000
Node Distribution	Uniform, Gaussian
Number of virtual rings	2 to 8
Operating frequency	868 MHz
Packet size	65 bytes
Operating voltage of nodes	3 V
Maximum number of payload aggregated in a packet	4

VIII. SIMULATION RESULTS

In this section, the SX1272 transceiver is used for simulation, and the simulation environment is similar to [38], [47]. Three schemes are considered: **Scheme I**, **Scheme II,** and **Scheme III**. One thousand nodes are distributed around the GW located in (0,0) for the aforementioned schemes. In **Scheme I** and **II**, nodes are placed following uniform distributions, while in **Scheme III**, nodes are placed following a Gaussian distribution with a mean of 0 and a standard deviation of 1.2. In **Scheme I and Scheme III**, rings are positioned following the "equidistant" distance spreading model, whereas in **Scheme II**, rings are positioned following the novel cluster formation technique proposed in Section VI. For all the schemes, 99% network connectivity is ensured. Simulation parameters can be found in Table 4.

A. ENERGY CONSUMPTION COMPARISON BETWEEN SCHEME I AND SCHEME II

Differences in transmit-energy consumptions between scheme I and scheme II are presented in Figure 5 for four virtual rings. In the case of DH routing, the most distant nodes from the GW are the critical nodes, and it can be seen that the nodes in the fourth ring consume the highest amount of energy among all the rings for both schemes. However, nodes in the third ring also consume the same amount of energy as the fourth ring nodes for both schemes in Figure 5. It can also happen with any selection of virtual ring numbers since nodes have to choose a particular transmission configuration from the available pool of transmission configurations and the transmission distance of a node is always greater than or equal to the distance between the GW and the node. In this case, while

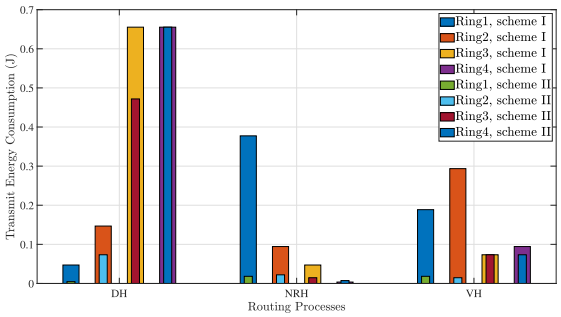

FIGURE 5. Transmit energy consumption for different routing processes.

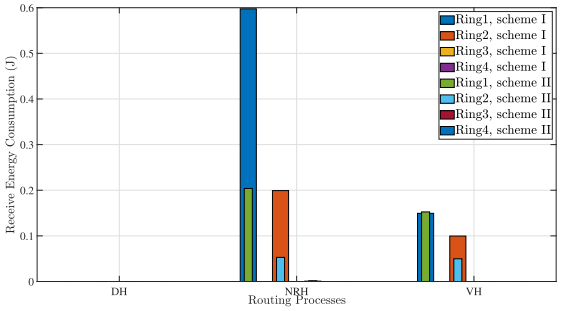

FIGURE 6. Receive energy consumption for different routing processes.

nodes in ring-3 and ring-4 have different distances from the GW, the transmission configuration choice remains the same for both rings as other transmission configurations fail to meet the required transmit distance.

In NRH routing, transmit energy consumption is reduced significantly in scheme II compared to scheme I. In VH routing, transmit energy consumption is reduced significantly for the nodes in ring-1 and ring-2.

Figure 6 represents the differences in received energy consumption between the schemes. As expected, a gradual increase in received energy consumption is observed for the nodes that are comparatively closer to the GW. Nevertheless, an attractive result is observed with scheme II when both the schemes are compared for nodes' received energy consumptions in ring-1 and ring-2. In VH routing, optimal ring-hop-combinations do not allow the nodes in ring-3 to receive any packets from any other nodes in the network for both schemes. Thus, no energy is consumed in the packet reception process for the nodes in ring-3 and ring-4.

Differences in nodes' total energy consumption in various rings are presented in Figure 7. Critical nodes are located in ring-1 for both schemes when NRH routing is considered. The critical nodes' energy consumptions are 0.9751 J and 0.2222 J for scheme I and scheme II, respectively. Thus, the new scheme offers a 77.21% improvement over the old scheme when NRH routing is considered. In VH routing, critical nodes are located in ring-2, and ring-1 for scheme I and scheme II, respectively, and the respective energy consumption rates are found to be 0.3932 J and 0.1709 J. The data represent 56.54% more energy consumption in scheme I compared to scheme II.

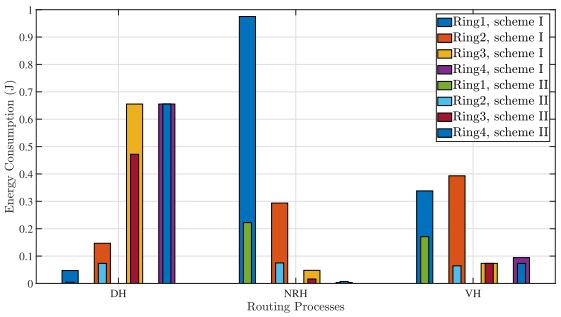

FIGURE 7. Total energy consumption for different routing processes.

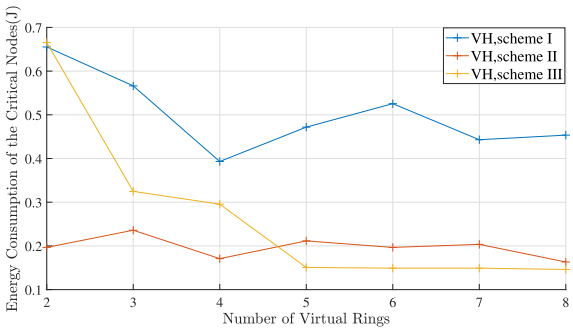

FIGURE 8. Energy consumption for VH routing and various numbers of virtual rings.

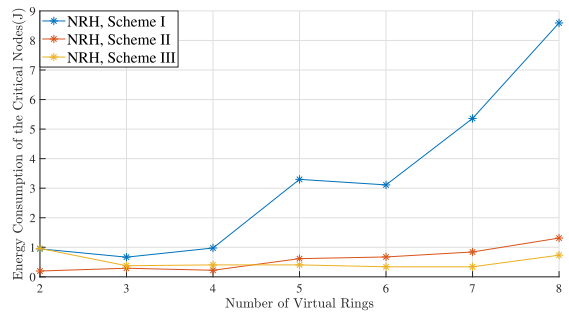

FIGURE 9. Energy consumption for NRH routing and various numbers of virtual rings.

B. VIRTUAL RINGS AND ENERGY CONSUMPTION IN SCHEME I, SCHEME II, AND SCHEME III

2 to 8 virtual rings are considered for comparison among the three schemes. Regardless of ring numbers, the energy consumption of critical nodes remains the same in DH routing for all the schemes. The impacts of the number of virtual rings in VH and NRH routing are shown in Figures 8 and 9.

It can be seen from Figure 8 that the energy consumption of critical nodes in scheme II and scheme III is significantly less compared to scheme I. The results for three and four virtual rings are discussed here. The energy consumptions of critical nodes are 0.5662 J, 0.2359 J, and 0.3248 J in scheme I, scheme II, and scheme III, respectively, for three virtual rings. 58.34% less energy is consumed in scheme II, and 42.64% less energy is consumed in scheme III than scheme I. When four virtual rings are considered, critical

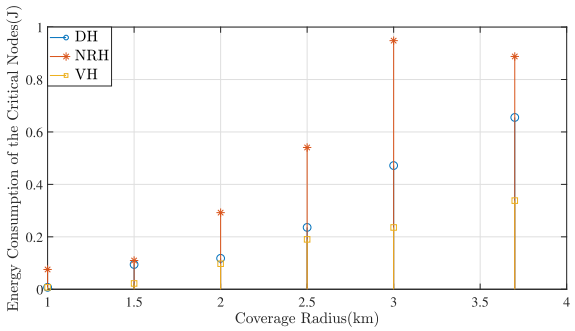

FIGURE 10. Energy consumption for different routing processes and coverage radius in Scheme I.

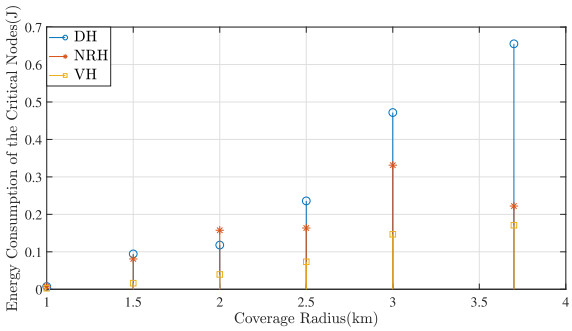

FIGURE 11. Energy consumption for different routing processes and coverage radius in Scheme II.

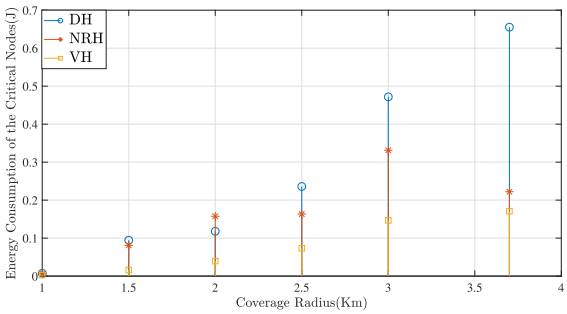

FIGURE 12. Energy consumption for different routing processes and coverage radius in Scheme III.

nodes' energy consumptions are 0.3932 J, 0.1709 J, and 0.2955 J in scheme I, scheme II, and scheme III. 56.54% and 24.85% less energy are consumed in scheme II and scheme III, respectively, compared against scheme I. For the case of NRH routing, Figure 9 shows that critical nodes' energy consumptions are 0.6658 J, 0.2909 J, and 0.3754 J for three virtual rings and 0.9751 J, 0.2222 J, and 0.4035 J for four virtual rings in scheme I, scheme II, and scheme III, respectively.

It is evident from Figures 8 and 9 that optimal VH routing uses substantially less energy than NRH routing. Nevertheless, when compared to scheme I, the proposed cluster formation (scheme III) significantly reduces the energy consumption of the critical nodes. Although we gave simulation results for $R \in [2, 8]$, it should be noted that the practical values of R are $2, 3, 4$, or 5. This is because, in addition to significantly increasing networking complexity, a larger number of rings may also result in an increase in packet loss. For $R = 3$ and above, VH routing-scheme III performed significantly better than VH routing-scheme I in Figure 9.

C. NETWORK COVERAGE AND ENERGY CONSUMPTION IN SCHEME I, SCHEME II, SCHEME III

Findings for scheme I are presented in Figure 10. NRH routing has the worst performance among the three routings regardless of coverage area. For a reduced network coverage area, critical nodes' energy expenditures are also reduced for both DH and VH routing. There is a significant difference in the energy consumption rate for different network coverage areas. It is observed that energy consumptions for smaller coverage areas are significantly reduced. For network coverage of 1 km, 1.5 km, 2 km, 2.5 km, 3 km, and 3.7 km and with the old scheme, critical nodes in VH routing consume 0%, 76.48%, 17.37%, 19.33%, 50.04%, and 48.41% less energy, respectively than DH routing while with the new cluster formation scheme, critical nodes in VH routing consume 63.51%, 82.84%, 66.44%, 68.89%, 68.89%, and 73.92% less energy consumption than DH routing.

Figure 11 shows that NRH routing with scheme II offers 7.69%, 56.25%, 31.86%, 56.15%, 87.44%, and 56.31% improvement over scheme I for network coverage of 1 km, 1.5 km, 2 km, 2.5 km, 3 km, and 3.7 km, respectively. In VH routing and for network coverage of 1 km, 1.5 km, 2 km, 2.5 km, 3 km, and 3.7 km, there are 0%, 58.19%, 18.53%, 47.65%, 79.48%, and 58.34% improvement with scheme II over the scheme I. When DH and VH routing are compared for scheme II and network coverage of 1 km, 1.5 km, 2 km, 2.5 km, 3 km, and 3.7 km, VH routing improves the energy efficiency by 0%, 92.16%, 49.32%, 47.65%, 79.48%, and 64%, respectively.

Figure 12 represents the performance of scheme III for different network coverage. Due to space limitations, we leave it for the readers to see the difference in DH, NRH, and VH routing performance.

D. PAYLOAD AGGREGATION AND ENERGY CONSUMPTION IN SCHEME I, SCHEME II AND SCHEME III

The impacts of payload aggregation on energy consumption are presented in Figure 13. $n_{\mathrm{DP}}^{[\mathrm{tx}]} = 1$ when payload aggregation is not considered and $n_{\mathrm{DP}}^{[\mathrm{tx}]} = 4$ when payload aggregation is considered. Energy consumption of critical nodes in scheme I, scheme II, and scheme-III can be reduced when payload aggregation is performed.

The four-virtual-rings case is picked as an example. Energy consumption of critical nodes for VH routing and

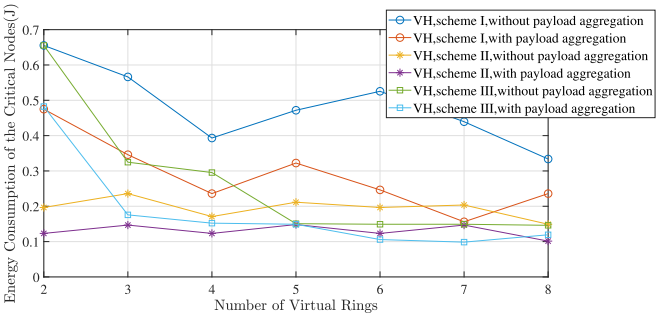

FIGURE 13. Impacts of payload aggregation on energy consumption.

scheme I is 0.3932 J when payload aggregation is not performed. Energy consumption reduces to 0.2359 J with payload aggregation. Energy consumptions of critical nodes are 0.1709 J and 0.2955 J in scheme II and scheme III, respectively, without payload aggregation. The energy savings in scheme II and scheme III, even without payload aggregation, are better than the energy savings achieved with payload aggregation in scheme I in some cases.

E. SUMMARY

Compared to Scheme I, which has a uniform distribution of nodes, the original Extended-DRESG performs significantly better with the Gaussian distribution (Scheme II). For uniform node distribution, Modified Extended-DRESG using the novel cluster formation strategy (Scheme III) performs significantly better than the original Extended-DRESG. The benefit margin could change, though, depending on how many virtual rings are selected. Since performance margins were previously discussed in this section, we will not repeat it here. One noteworthy finding was that, in certain scenarios, the Extended-DRESG modification provides performance that is superior to the original Extended-DRESG with payload aggregation. However, regardless of the schemes, the benefits of multi-hop routing can be significantly diminished for smaller coverage areas.

IX. CONCLUSION

In this research, we demonstrate how a Gaussian distribution can be used to describe LoRa networks at their maximum capacity. Although it is not unusual to see networks with uniform distribution, this is because some applications may not use the full network capacity. We then investigate the impact of packet forwarding structure on nodes' energy consumption to better understand the routing performance for various node distributions. After conducting the analysis, we create an algorithm that can be utilized to identify the best ring placements and ring-hop combinations for the Extended-DRESG routing scheme we had previously presented. Following that, a straightforward cluster formation algorithm for networks with evenly dispersed LoRa networks is developed using the observations made in this paper. The effectiveness of the new cluster formation strategy in improving network lifetime is shown by simulation results.

REFERENCES

[1] M. Centenaro, L. Vangelista, A. Zanella, and M. Zorzi, "Long-range communications in unlicensed bands: The rising stars in the IoT and smart city scenarios," *IEEE Wireless Commun.*, vol. 23, no. 5, pp. 60–67, Oct. 2016.

[2] A. A. A. Boulogeorgos, P. D. Diamantoulakis, and G. K. Karagiannidis, "Low power wide area networks (LPWANs) for Internet of Things (IoT) applications: Research challenges and future trends," 2016, *arXiv:1611.07449*.

[3] G. Loubet, A. Takacs, and D. Dragomirescu, "Implementation of a battery-free wireless sensor for cyber-physical systems dedicated to structural health monitoring applications," *IEEE Access*, vol. 7, pp. 24679–24690, 2019.

[4] G. Yang and H. Liang, "A smart wireless paging sensor network for elderly care application using LoRaWAN," *IEEE Sensors J.*, vol. 18, no. 22, pp. 9441–9448, Nov. 2018.

[5] M. Rizzi, P. Ferrari, A. Flammini, and E. Sisinni, "Evaluation of the IoT LoRaWAN solution for distributed measurement applications," *IEEE Trans. Instrum. Meas.*, vol. 66, no. 12, pp. 3340–3349, Dec. 2017.

[6] C. Ebi, F. Schaltegger, A. Rüst, and F. Blumensaat, "Synchronous LoRa mesh network to monitor processes in underground infrastructure," *IEEE Access*, vol. 7, pp. 57663–57677, 2019.

[7] I. F. Priyanta, F. Golatowski, T. Schulz, and D. Timmermann, "Evaluation of LoRa technology for vehicle and asset tracking in smart harbors," in *Proc. 45th Annu. Conf. IEEE Ind. Electron. Soc.*, vol. 1, Oct. 2019, pp. 4221–4228.

[8] J. Haxhibeqiri, F. Van den Abeele, I. Moerman, and J. Hoebeke, "LoRa scalability: A simulation model based on interference measurements," *Sensors*, vol. 17, no. 6, p. 1193, 2017.

[9] M. Rizzi, P. Ferrari, A. Flammini, E. Sisinni, and M. Gidlund, "Using LoRa for industrial wireless networks," in *Proc. IEEE 13th Int. Workshop Factory Commun. Syst. (WFCS)*, May 2017, pp. 1–4.

[10] J. Petäjäjärvi, K. Mikhaylov, R. Yasmin, M. Hämäläinen, and J. Iinatti, "Evaluation of LoRa LPWAN technology for indoor remote health and wellbeing monitoring," *Int. J. Wireless Inf. Netw.*, vol. 24, pp. 153–165, Feb. 2017.

[11] A. P. A. Torres, C. B. Da Silva, and H. T. Filho, "An experimental study on the use of LoRa technology in vehicle communication," *IEEE Access*, vol. 9, pp. 26633–26640, 2021.

[12] "LoRa Alliance." 2023. [Online]. Available: https://lora-alliance.org/

[13] K. Mikhaylov, J. Petaejaejaervi, and T. Haenninen, "Analysis of capacity and scalability of the LoRa low power wide area network technology," in *Proc. 22nd Eur. Wireless Conf.*, May 2016, pp. 1–6.

[14] Q. Song, X. Lagrange, and L. Nuaymi, "An analytical model for S-ALOHA performance evaluation in M2M networks," in *Proc. IEEE Int. Conf. Commun. (ICC)*, May 2017, pp. 1–7.

[15] U. Reza, P. Kulkarni, and M. Sooriyabandara, "Low power wide area networks: An overview," *IEEE Commun. Surveys Tuts.*, vol. 19, no. 2, pp. 855–873, 2nd Quart., 2017.

[16] K. H. Lam, C. C. Cheung, and W. C. Lee, "RSSI-based LoRa localization systems for large-scale indoor and outdoor environments," *IEEE Trans. Veh. Technol.*, vol. 68, no. 12, pp. 11778–11791, Dec. 2019.

[17] F. Lemic, A. Behboodi, J. Famaey, and R. Mathar, "Location-based discovery and vertical handover in heterogeneous low-power wide-area networks," *IEEE Internet Things J.*, vol. 6, no. 6, pp. 10150–10165, Dec. 2019.

[18] O. Georgiou, C. Psomas, C. Skouroumounis, and I. Krikidis, "Optimal non-uniform deployments of LoRa networks," *IEEE Wireless Commun. Lett.*, vol. 9, no. 11, pp. 1919–1923, Nov. 2020.

[19] M. Jouhari, N. Saeed, M. S. Alouini, and E. M. Amhoud, "A survey on scalable LoRaWAN for massive IoT: Recent advances, potentials, and challenges," *IEEE Commun. Surveys Tuts.*, vol. 25, no. 3, pp. 1841–1876, 3rd Quart., 2023.

[20] P. Maurya, A. Singh, and A. A. Kherani, "A review: Spreading factor allocation schemes for LoRaWAN," *Telecommun. Syst.*, vol. 80, no. 3, pp. 449–468, 2022.

[21] R. Subbaraman, Y. Guntupalli, S. Jain, R. Kumar, K. Chintalapudi, and D. Bharadia, "BSMA: Scalable LoRa networks using full duplex gateways," in *Proc. 28th Annu. Int. Conf. Mobile Comput. Netw.*, Oct. 2022, pp. 676–689.

[22] M. Xhonneux, J. Tapparel, A. Balatsoukas-Stimming, A. Burg, and O. Afisiadis, "A maximum-likelihood-based two-user receiver for LoRa chirp spread-spectrum modulation," *IEEE Internet Things J.*, vol. 9, no. 22, pp. 22993–23007, Nov. 2022.

[23] D. Todoli-Ferrandis, J. Silvestre-Blanes, V. Sempere-Payá, and S. Santonja-Climent, "Adaptive beacon period configurator for scalable LoRaWAN downlink applications," *IEEE Access*, vol. 11, pp. 83627–83638, 2023.

[24] A. Farhad, D. H. Kim, and J. Y. Pyun, "Resource allocation to massive Internet of Things in LoRaWANs," *Sensors*, vol. 20, no. 9, p. 2645, 2020.

[25] J. T. Lim and Y. Han, "Spreading factor allocation for massive connectivity in LoRa systems," *IEEE Commun. Lett.*, vol. 22, no. 4, pp. 800–803, Apr. 2018.

[26] Y. Hou, Z. Liu, and D. Sun, "A novel MAC protocol exploiting concurrent transmissions for massive LoRa connectivity," *J. Commun. Netw.*, vol. 22, no. 2, pp. 108–117, 2020.

[27] A. Mahmood, E. Sisinni, L. Guntupalli, R. Rondón, S. A. Hassan, and M. Gidlund, "Scalability analysis of a LoRa network under imperfect orthogonality," *IEEE Trans. Ind. Informat.*, vol. 15, no. 3, pp. 1425–1436, Mar. 2019.

[28] Q. Guo, F. Yang, and J. Wei, "Experimental evaluation of the packet reception performance of LoRa," *Sensors*, vol. 21, no. 4, p. 1071, 2021.

[29] S. Narieda, T. Fujii, and K. Umebayashi, "Energy constrained optimization for spreading factor allocation in LoRaWAN," *Sensors*, vol. 20, no. 16, p. 4417, 2020.

[30] B. Paul, "A novel mathematical model to evaluate the impact of packet re-transmissions in LoRaWAN," *IEEE Sens. Lett.*, vol. 4, no. 5, pp. 1–4, May 2020.

[31] V. Toro-Betancur, G. Premsankar, C. F. Liu, M. Słabicki, M. Bennis, and M. Di Francesco, "Learning how to configure LoRa networks with no regret: A distributed approach," *IEEE Trans. Ind. Informat.*, vol. 19, no. 4, pp. 5633–5644, Apr. 2023.

[32] J. F. Schmidt, U. Schilcher, S. S. Borkotoky, and C. A. Schmidt, "Energy consumption in LoRa IoT: Benefits of adding relays to dense networks," in *Proc. IEEE Symp. Comput. Commun. (ISCC)*, Jun. 2022, pp. 1–6.

[33] B. Błaszczyszyn and P. Mühlethaler, "Analyzing LoRa long-range, low-power, wide-area networks using stochastic geometry," in *Proc. 12th EAI Int. Conf. Perform. Eval. Methodol. Tools*, Mar. 2019, pp. 119–126.

[34] S. Feng, J. Chen, and Z. Zhao, "Cost effective routing in large-scale multi-hop LoRa networks," in *Proc. IEEE Conf. Comput. Commun. Workshops (INFOCOM WKSHPS)*, May, 2022, pp. 1–6.

[35] Y. H. Tehrani, A. Amini, and S. M. Atarodi, "A tree-structured LoRa network for energy efficiency," *IEEE Internet Things J.*, vol. 8, no. 7, pp. 6002–6011, Apr. 2021.

[36] N. A. Pantazis, S. A. Nikolidakis, and D. D. Vergados, "Energy-efficient routing protocols in wireless sensor networks: A survey," *IEEE Commun. Surveys Tuts.*, vol. 15, no. 2, pp. 551–591, 2nd Quart., 2013.

[37] J. Hao, B. Zhang, and H. T. Mouftah, "Routing protocols for duty cycled wireless sensor networks: A survey," *IEEE Commun. Mag.*, vol. 50, no. 12, pp. 116–123, Dec. 2012.

[38] S. Barrachina-Muñoz, B. Bellalta, T. Adame, and A. Bel, "Multi-hop communication in the uplink for LPWANs," *Comput. Netw.*, vol. 123, pp. 153–168, Aug. 2017.

[39] H. C. Lee and K. H. Ke, "Monitoring of large-area IoT sensors using a LoRa wireless mesh network system: Design and evaluation," *IEEE Trans. Instrum. Meas.*, vol. 67, no. 9, pp. 2177–2187, Sep. 2018.

[40] C. H. Liao, G. Zhu, D. Kuwabara, M. Suzuki, and H. Morikawa, "Multi-hop LoRa networks enabled by concurrent transmission," *IEEE Access*, vol. 5, pp. 21430–21446, 2017.

[41] G. Zhu, C. H. Liao, T. Sakdejayont, I. W. Lai, Y. Narusue, and H. Morikawa, "Improving the capacity of a mesh LoRa network by spreading-factor-based network clustering," *IEEE Access*, vol. 7, pp. 21584–21596, 2019.

[42] M. O. Farooq, "Clustering-based layering approach for uplink multi-hop communication in LoRa networks," *IEEE Netw. Lett.*, vol. 2, no. 3, pp. 132–135, Sep. 2020.

[43] M. S. Aslam et al., "Exploring multi-hop LoRa for green smart cities," *IEEE Netw.*, vol. 34, no. 2, pp. 225–231, Mar./Apr. 2020.

[44] R. P. Centelles, F. Freitag, R. Meseguer, and L. Navarro, "Beyond the star of stars: An introduction to multihop and mesh for LoRa and LoRaWAN," *IEEE Pervasive Comput.*, vol. 20, no. 2, pp. 63–72, Apr.–Jun. 2021.

[45] P. Tian, C. A. Boano, X. Ma, and J. Wei, "LoRaHop: Multi-hop support for LoRaWAN uplink and downlink messaging," *IEEE Internet Things J.*, vol. 10, no. 17, pp. 15376–15392, Sep. 2023.

[46] M. R. Islam, M. Bokhtiar-Al-Zami, B. Paul, R. Palit, J. C. Grégoire, and S. Islam, "Performance evaluation of multi-hop LoRaWAN," *IEEE Access*, vol. 11, pp. 50929–50945, 2023.

[47] B. Paul, "A novel energy-efficient routing scheme for LoRa networks," *IEEE Sensors J.*, vol. 20, no. 15, pp. 8858–8866, Aug. 2020.

[48] M. Vaezi et al., "Cellular, wide-area, and non-terrestrial IoT: A survey on 5G advances and the road toward 6G," *IEEE Commun. Surveys Tuts.*, vol. 24, no. 2, pp. 1117–1174, 2nd Quart., 2022.

[49] "Enhanced relays for energy efficiency and extensive coverage," 3GPP, Sophia Antipolis, France, Rep. TR 22.866, Feb. 2019.

[50] S. Murugaanandam and V. Ganapathy, "Reliability-based cluster head selection methodology using fuzzy logic for performance improvement in WSNs," *IEEE Access*, vol. 7, pp. 87357–87368, 2019.

[51] J. Kruse, S. Mandelli, and S. R. Khosravirad, "QoS-aware wireless sensor networks: Reliability and low-latency for heterogeneous Industry 4.0," in *Proc. IEEE 93rd Veh. Technol. Conf. (VTC-Spring)*, Apr. 2021, pp. 1–5.

[52] Q. V. Khanh, A. Chehri, N. M. Quy, N. D. Han, and N. T. Ban, "Innovative trends in the 6G era: A comprehensive survey of architecture, applications, technologies, and challenges," *IEEE Access*, vol. 11, pp. 39824–39844, 2023.

[53] W. Yu, Y. Chen, L. Wan, X. Zhang, P. Zhu, and X. Xu, "An energy optimization clustering scheme for multi-hop underwater acoustic cooperative sensor networks," *IEEE Access*, vol. 8, pp. 89171–89184, 2020.

[54] P. Phibbs and S. Lentz, "The implementation of the NEPTUNE Canada backbone network," in *Proc. IEEE OCEANS*, Sep. 2007, pp. 1–5.

[55] J. Rice et al., "Evolution of SeaWeb underwater acoustic networking," in *Proc. MTS/IEEE Conf. Exhibit.*, vol. 3, Sep. 2000, pp. 2007–2017.

[56] M. Grund, L. Freitag, J. Preisig, and K. Ball, "The PLUSNet underwater communications system: Acoustic telemetry for undersea surveillance," in *Proc. IEEE OCEANS*, Sep. 2006, pp. 1–5.

[57] G. Giambene and K. Korre, "LoRa-based system for IoT applications via HAPS in remote areas," in *Proc. IEEE Int. Conf. Softw. Telecommun. Comput. Netw. (SoftCOM)*, Sep. 2022, pp. 1–6.

[58] M. A. Ullah, K. Mikhaylov, and H. Alves, "Enabling mMTC in remote areas: LoRaWAN and LEO satellite integration for offshore wind farm monitoring," *IEEE Trans. Ind. Informat.*, vol. 18, no. 6, pp. 3744–3753, Jun. 2022.

[59] R. Marini and G. Cuozzo, "A comparative performance analysis of LoRaWAN in two frequency spectra: EU868 MHz and 2.4 GHz," in *Proc. IEEE Joint Eur. Conf. Netw. Commun. 6G Summit (EuCNC/6G Summit)*, Jun. 2023, pp. 1–6.

[60] P. Masek et al., "Performance analysis of different LoRaWAN frequency bands for mMTC scenarios," in *Proc. IEEE 45th Int. Conf. Telecommun. Signal Process. (TSP)*, Jul. 2022, pp. 417–420.

[61] G. A. Akpakwu, B. J. Silva, G. P. Hancke, and A. M. Abu-Mahfouz, "A survey on 5G networks for the Internet of Things: Communication technologies and challenges," *IEEE Access*, vol. 6, pp. 3619–3647, 2018.

[62] "Datasheet SX1272/73–860 MHz to 1020 MHz low power long range transceiver," Datasheet, Semtech, SX1272, Camarillo, CA, USA, Mar. 2015,

[63] A. Alsohaily, E. Sousa, A. J. Tenenbaum, and I. Maljevic, "LoRaWAN radio interface analysis for North American frequency band operation," in *Proc. IEEE 28th Annu. Int. Symp. Pers. Indoor, Mobile Radio Commun. (PIMRC)*, Oct. 2017, pp. 1–6.

[64] S. Aggarwal and A. Nasipuri, "Improving scalability of LoRaWAN networks by spreading factor distribution," in *Proc. IEEE SoutheastCon*, Mar. 2021, pp. 1–7.